Second Order Perturbation Analysis of 1D Linearly Polarized Alfven Wave

Zesen Huang

March 2, 2020

1 Theoretical Setup

1.1 MHD Equations

$$\frac{\partial \rho}{\partial t} + \nabla \cdot (\rho \boldsymbol{u}) = 0 \tag{1}$$

$$\rho \left[\frac{\partial \boldsymbol{u}}{\partial t} + (\boldsymbol{u} \cdot \nabla)\boldsymbol{u} \right] = -\nabla p + \frac{1}{\mu}(\nabla \times \boldsymbol{B}) \times \boldsymbol{B} \tag{2}$$

$$\frac{\partial \boldsymbol{B}}{\partial t} = \nabla \times (\boldsymbol{u} \times \boldsymbol{B}) \tag{3}$$

$$\nabla \cdot \boldsymbol{B} = 0 \tag{4}$$

$$p = p(\rho) = p^{\gamma} \tag{5}$$

$$c_s = \sqrt{(\frac{\partial p}{\partial \rho})_s} \tag{6}$$

1.2 Initial Conditions and Perturbation Conditions

In this analysis, only 1 dimension is considered, i.e.

$$f \sim f(x,t),\ \nabla = \hat{\boldsymbol{x}}\partial_x \tag{7}$$

The initial perturbation is along y direction and is set as linearly polarized alfvenic perturbation i.e. for the first order perturbation only u_{1y} and B_{1y} are presented, neither first order u_{1x} nor ρ_1 are presented.

$$\boldsymbol{u} = \boldsymbol{u}_1 + \boldsymbol{u}_2 = u_{1y}\hat{\boldsymbol{y}} + u_{2x}\hat{\boldsymbol{x}} + u_{2y}\hat{\boldsymbol{y}} + u_{2z}\hat{\boldsymbol{z}} \tag{8}$$

$$\boldsymbol{B} = \boldsymbol{B}_0 + \boldsymbol{B}_1 + \boldsymbol{B}_2 = B_0\hat{\boldsymbol{x}} + B_{1y}\hat{\boldsymbol{y}} + B_{2y}\hat{\boldsymbol{y}} + B_{2z}\hat{\boldsymbol{z}} \tag{9}$$

$$\rho = \rho_0 + \rho_2 \tag{10}$$

2 First Order Linearization

$$\frac{\partial \rho_1}{\partial t} + \rho_0 \frac{\partial u_1 x}{\partial x} = 0 \tag{11}$$

$$\rho_0 \frac{\partial u_{1x}}{\partial t} = -c_s^2 \frac{\partial \rho}{\partial x} \tag{12}$$

$$\rho_0 \frac{\partial u_{1y}}{\partial t} = \frac{B_0}{\mu} \partial_x B_{1y} \tag{13}$$

$$\frac{\partial B_{1y}}{\partial t} = B_0 \partial_x u_{1y} \tag{14}$$

$$\rho_0 \frac{\partial u_{1z}}{\partial t} = \frac{B_0}{\mu} \partial_x B_{1z} \tag{15}$$

$$\frac{\partial B_{1z}}{\partial t} = B_0 \partial_x u_{1z} \tag{16}$$

Together (11)-(16) forms three groups of decoupled wave equation, with (11)-(12) sound wave, (13)-(14) Alfven wave ($\hat{\boldsymbol{y}}$) and (15)-(16) Alfven wave ($\hat{\boldsymbol{z}}$). It is evident that in our case, only (13)-(14) deserves further consideration, nevertheless, it is worth pointing out that y and z direction decouples with each other and with x direction, hence we would ignore z direction for the rest of this analysis.

Obviously (13)-(14) yields:

$$\frac{\partial^2}{\partial t^2} u_{1y} = \frac{B_0^2}{\mu \rho_0} \frac{\partial^2}{\partial x^2} u_{1y} \tag{17}$$

$$\frac{\partial^2}{\partial t^2} B_{1y} = \frac{B_0^2}{\mu \rho_0} \frac{\partial^2}{\partial x^2} B_{1y} \tag{18}$$

Needlessly to say this yields:

$$u_{1y} = u_{1y}(x \pm v_{a0}t),\ B_{1y} = B_{1y}(x \pm v_{a0}t) \tag{19}$$

where $v_{a0} = \frac{B_0}{\sqrt{\mu\rho_0}}$ is the unperturbed alfven wave velocity. And the fluctuation amplitude is related by:

$$\tilde{u_{1y}} = -\frac{< \boldsymbol{B}_0 \cdot \hat{\boldsymbol{k}} >}{\sqrt{\mu\rho_0}}\tilde{B_{1y}} \tag{20}$$

It is obvious that first order analysis is trivial so we would stop here.

3 Second Order Linearization

Now we will begin second order analysis

$$\frac{\partial\rho_2}{\partial t} + \rho_0\frac{\partial u_{2x}}{\partial x} = 0 \tag{21}$$

$$\rho_0\frac{\partial u_{2x}}{\partial t} = -c_s^2\frac{\partial\rho_2}{\partial x} - \frac{\partial}{\partial x}\left(\frac{B_1^2}{2\mu}\right) \tag{22}$$

$$\rho_0\frac{\partial u_{2y}}{\partial t} = \frac{B_0}{\mu}\partial_x B_{2y} \tag{23}$$

$$\frac{\partial B_{2y}}{\partial t} = B_0\partial_x u_{2y} \tag{24}$$

Obviously the second order alfvenic perturbation in y direction is trivial. We will hence focus on (21)-(22) for the rest of this analysis. Note that there is an **untrivial new term** in the sound wave perturbation (22), which is $\partial_x(B_1^2/2\mu)$

Equations (21)-(22) will merge into:

$$\frac{\partial^2\rho_2}{\partial t^2} - c_s^2\frac{\partial^2\rho_2}{\partial x^2} = \frac{\partial^2}{\partial x^2}\left(\frac{B_1^2}{2\mu}\right) \tag{25}$$

Note that the right-hand-side of this equation is the magnetic pressure, effectively a source term.

Before proceeding any further, for comparison, we shall discuss the second order analysis of sound wave for a little bit. Similar equation yields from second order analysis of sound wave, which is:

$$\frac{\partial^2\rho_2}{\partial t^2} - c_s^2\frac{\partial^2\rho_2}{\partial x^2} = \frac{c_s^2}{\rho_0}\overbrace{(1 + \frac{\rho_0}{c_s}\frac{dc_s}{d\rho})}^{G}\frac{\partial^2\rho_1^2}{\partial x^2} = \frac{\partial^2}{\partial x^2}(\rho_0 v_1^2 + \frac{\partial^2 p}{\partial\rho^2}\frac{\rho_1^2}{2}) \tag{26}$$

Similarly, RHS of both equations are pressure. So what are these equations? They are actually forced oscillation! Before going back to our analysis of Alfvenic analysis, we shall extract more information from the sound wave analysis.

The solution of the a normal sound wave is:

$$\rho_1 = \rho_1(x \pm c_s t),\ v_1 = v_1(x \pm c_s t) \tag{27}$$

Given that LHS of (26) is a wave equation with phase velocity of c_s, this equation is always resonant. The solution to (26) is a bit exotic (to me):

$$\rho_2 = \frac{c_s t}{2\rho_0} G \frac{\partial \rho_1^2}{\partial x} = \frac{c_s t}{2\rho_0}(1 + \frac{\rho_0}{c_s}\frac{dc_s}{d\rho})\frac{\partial \rho_1^2}{\partial x} \tag{28}$$

Note the t in (28), ρ_2 grows linearly with respect to time. Hence this is an unstable solution, which leads to the formation of hydrodynamic shock. Now we shall return to our analysis of alfven wave.

4 Solution to Second Order 1-D Linearly Polarized Alfvenic Fluctuation

Now return to (25)

$$\frac{\partial^2 \rho_2}{\partial t^2} - c_s^2 \frac{\partial^2 \rho_2}{\partial x^2} = \frac{\partial^2}{\partial x^2}\left(\frac{B_1^2}{2\mu}\right)$$

Note that $B_1 = B_1(x - v_{a0}t)$ hence there are two completely different cases for (25). The trivial case is when $c_s \neq v_a$, the solution to (25) is a solution to forced oscillation (ignore damping in our case). The non-trivial case is when $c_s = v_a$, the forced-oscillation resonates. In this case, the solution will share the same form with the sound wave's. We shall discuss the trivial case first and then the non-trivial case.

4.1 Non-Resonant Solution

Take $B_1 = \tilde{B_{1y}} cos[k(x - v_{a0}t)]$ and guess $\rho_2 = \tilde{\rho_2} cos[2k(x - v_{a0}t)]$. The solution to (25) yields:

$$\rho_2 = -\frac{\tilde{B_{1y}}^2}{4\mu(c_s^2 - v_{a0}^2)} cos[2k(x - v_{a0}t)] \tag{29}$$

From (21):

$$\frac{\partial \rho_2}{\partial t} + \rho_0 \frac{\partial u_{2x}}{\partial x} = 0$$

We yield:

$$u_{2x} = -\frac{v_{a0}\tilde{B_{1y}}^2}{4\mu\rho_0(c_s^2 - v_{a0}^2)} cos[2k(x - v_{a0}t)] \tag{30}$$

One of the most important features of the wave steepening is its waveform deformation and the subsequent formation of discontinuity. The actual phase velocity of 1-D Alfven wave is $v_\varphi = u_x + v_a$. Hence the disturbance of phase velocity is $\delta v_\varphi = u_{2x} + \delta v_a$. Disturbance of v_a is:

$$v_a = \frac{B_0}{\sqrt{\mu\rho}} = \frac{B_0}{\sqrt{\mu\rho_0}}\left[1 - \frac{1}{2}\frac{\rho_2}{\rho_0} + o(\frac{\rho_2}{\rho_0})\right] \approx v_{a0}(1 - \frac{1}{2}\frac{\rho_2}{\rho_0}) \tag{31}$$

This yields:

$$\delta v_\varphi = -\frac{v_{a0}\tilde{B_{1y}}^2}{8\mu\rho_0(c_s^2 - v_{a0}^2)} cos[2k(x - v_{a0}t)] \tag{32}$$

Looking at (32) we could see that the shape of the wave steepening is determined by $sgn(c_s^2 - v_{a0}^2)$. A more detailed analysis would be conducted in the simulation results section.

4.2 Resonant Solution

For the non-trivial case ($v_a = c_s$), we will substitute c_s with v_a. (25) now becomes:

$$\frac{\partial^2\rho_2}{\partial t^2} - v_{a0}^2\frac{\partial^2\rho_2}{\partial x^2} = \frac{\partial^2}{\partial x^2}\left(\frac{B_1^2}{2\mu}\right) \tag{33}$$

with

$$B_1 = B_1(x - v_{a0}t) = B_1(\varphi) \tag{34}$$

The solution is:

$$\rho_2 = -\frac{t}{4\mu v_{a0}}\frac{\partial B_1^2}{\partial\varphi} \tag{35}$$

Again with (21), yields;

$$u_{2x} = \frac{B_1^2}{4\mu\rho_0 v_{a0}} - \frac{t}{4\mu\rho_0}\frac{\partial B_1^2}{\partial\varphi} \tag{36}$$

There are two notable features here:

- ρ_2, u_{2x} grows linearly with respect to time in same speed.
- Amplitude of u_{2x} and ρ_2 has a factor of v_{a0}/ρ_0 difference.
- u_{2x} has an offset (proportional to B_1^2)

We shall verify these two features together with the features of non-resonant case using simulation in the following section.

5 Simulation Results

5.1 Non-Resonant Case

Let's start by verifying the behavior of B_{1y}, $\delta\rho_2$ and u_{2x}. Figure 1 is a time elapse of B_{1y}, $\delta\rho_2$ and u_{2x} at fixed point $x = 0$.

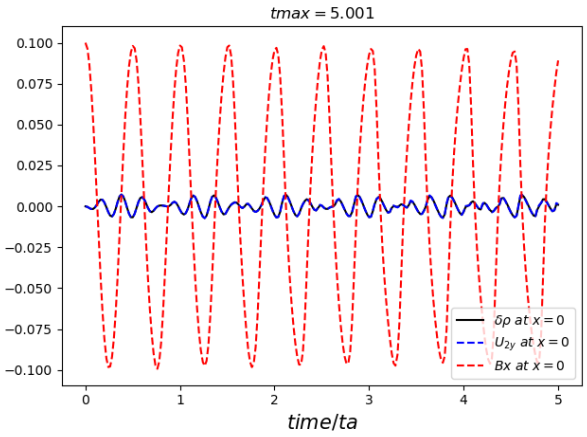

Figure 1: Time elapse of B_{1y}, $\delta\rho_2$ and u_{2x} at fixed point $x = 0$

It can be seen from figure 1 that result of second order analysis (29) and (30) captures features of frequency and amplitude with reasonable accuracy. For example, B_{1y} and $\delta\rho_2$ are supposed to in phase with each other (they overlap each other in figure 1). Moreover, B_{1y} and $\delta\rho_2$ are also supposed to have amplitude of B_{1y}^2 and have frequency doubled of B_{1y}'s frequency, which is captured incredibly well as can be found in figure 1. However, based on the result of the second order analysis, the fluctuation amplitude of B_{1y} and $\delta\rho_2$ are supposed to stay constant, as opposed to the simulation result, which obviously comprise a lower order wave packet. It is worth noting that the wave steepening speed is over 2 times faster than the speed expected from a order of magnitude analysis of v_φ. This might be caused by the unexpected amplitude fluctuation of both B_{1y} and $\delta\rho_2$. One might guess this comes from higher order effects.

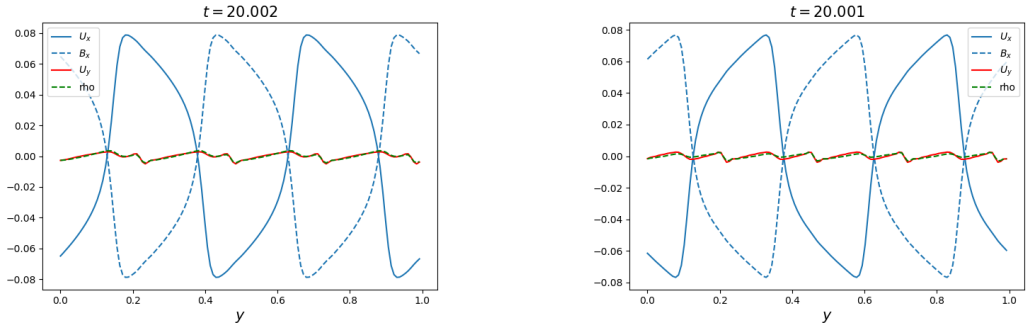

(a) $B_0 = 1.0, t = 20t_a$
Cliff at left

(b) $B_0 = 1.0, t = 20t_a$
Cliff at right

Figure 2: Different Shape of Steepening

From (32)

$$\delta v_\varphi = -\frac{v_{a0}\tilde{B_{1y}}^2}{8\mu\rho_0(c_s^2 - v_{a0}^2)} cos[2k(x - v_{a0}t)]$$

we can estimate the shape of the steepening by $sgn(v_a^2 - c_s^2)$. When $v_a^2 < c_s^2$ (Note $c_s^2 = \gamma p_0/\rho_0 = 5/3, v_{a0}^2 = B_0/\sqrt{\mu\rho_0} = B_0$), i.e. $\delta v_\varphi < 0$, the phase velocity at $\varphi = k(x - v_{a0}t) = 0$ is smaller than

the phase velocity at $\varphi = k(x - v_{a0}t) = \pi/2$. The phase velocity difference is:

$$\Delta v_\varphi = v_\varphi(\varphi = 0) - v_\varphi(\varphi = \pi/2) = 2 * -\frac{v_{a0}\tilde{B_{1y}}^2}{8\mu\rho_0(c_s^2 - v_{a0}^2)} \tag{37}$$

As a result, the peak of B_{1y} will move left relative to the zeros and forms a cliff (discontinuity) at the left side as a consequence (See Figure 2.a). Similar analysis when $v_a^2 > c_s^2$ will yield the result that a cliff (discontinuity) will be form at the right side (See Figure 2.b).

5.2 Resonant Case

To test the correctness of (35), it is convenient to take a average of ρ_2 (in the following analysis, assume $B_1 = \tilde{B_{1y}}cos(k\varphi) = \tilde{B_{1y}}cos[k(x - v_{a0}t)]$):

$$< |\rho_2| >_x = -\frac{t}{4\mu v_{a0}} < |\frac{\partial B_1^2}{\partial \varphi}| >_x = \frac{t\tilde{B_{1y}^2}}{4\mu v_{a0}} * k * < |sin2\varphi| >_\varphi = \frac{t\tilde{B_{1y}^2}}{4\mu v_{a0}} * k * \frac{2}{\pi} \tag{38}$$

Obviously $< |\rho_2| >_x$ is estimated to increase with time linearly. To produce the resonant case, B_0 is set to 1.291 ($\sqrt{\gamma} = \sqrt{5/3} \approx 1.291$), an example result is presented in Figure 3.a and Figure 3.b. In this run $\tilde{B_{1y}}$ is 0.01 and k is 4π. The result displays an incredibly clear and stable linear growth with respect to time (both in 3.a and the wave packet in 3.b). Both ρ_2 and u_{2y} saturate at about 15 t_a and hence this resonance seems to be an **amazingly fast way to convert magnetic energy to kinetic energy**. To compare the theoretical growth rate and the simulated growth rate, a linear fit is done using the data of the first 5 Alfven time ($t_a = L_y/v_{a0}$) and the result is $b_{sim} = 1.505 \times 10^{-4}$. For comparison, the theoretical growth rate is ($\tilde{B_{1y}} = 0.01, k = 4\pi, \mu = 1, v_{a0} = B_0/\sqrt{\mu\rho_0} = \sqrt{\gamma}$): $b_{the} = 1.549 \times 10^{-4}$. The relative difference between the theoretical growth rate and the simulation growth rate is about 3%, which may come from higher order effect. More simulation runs shows that this growth rate error changes with regard to k and $\tilde{B_{1y}}$, further investigation should be taken on this.

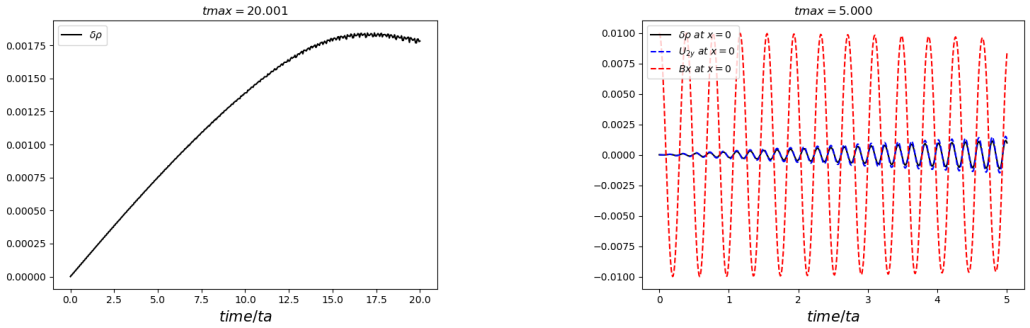

(a) $\delta\rho_{2,rms}$

(b) Time elapse of B_{1y}, $\delta\rho_2$ and u_{2x}

Figure 3: $\delta\rho_{2,rms}$ and Time elapse of B_{1y}, $\delta\rho_2$ and u_{2x} at fixed point $x = 0$ (first $5t_a$), Small amplitude $\tilde{B_{1y}} = 0.01$

Note that in figure 3b, the amplitude of u_{2x} is slightly larger than $\delta\rho$ and the difference increases with time. This comes from a factor of $v_{a0}/\rho_0 \approx 1.291$ difference of growing term between u_{2x} and $\delta\rho$ in (35) and (36).

The offset of u_{2x} is not obvious in Figure 3 (Small Amplitude Wave) but can be rather obvious if we increase $\tilde{B_{1y}}$. Figure 4 is a large amplitude version of this simulation (resonance). In Figure 4, $\tilde{B_{1y}}$ is set to 0.5. It can be seen in 4.b that there is an very obvious symmetry breaking in u_{2x} and ρ_2, even though the sign is different from what is expected from (36). And it is worth noting that the growth saturates extremely fast — at $0.4t_a$!

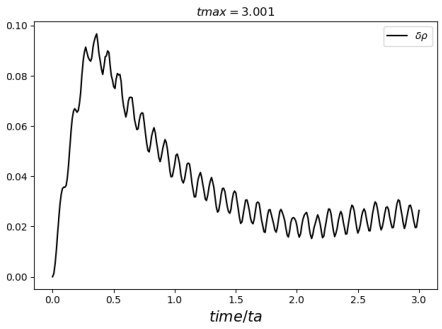

(a) $\delta\rho_{2,rms}$

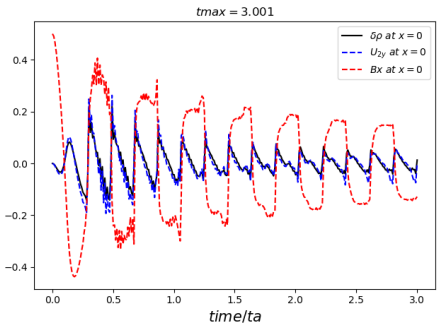

(b) Time elapse of B_{1y}, $\delta\rho_2$ and u_{2x}

Figure 4: $\delta\rho_{2,rms}$ and Time elapse of B_{1y}, $\delta\rho_2$ and u_{2x} at fixed point $x = 0$, Large Amplitude ($\tilde{B_{1y}} = 0.5$)

6 Movie Links

Time-Lapse Movie Link:

Small Amplitude Resonance

Large Amplitude Resonance

7 Supplement Materials

7.1 Detailed Analysis on Resonance Growth Rate

A more detailed analysis is conducted concerning the linear growth rate in resonance situation. A linear growth rate estimated using sliding window is presented in figure 5. In this case, the magnetic field perturbation $\tilde{B_{1y}}$ is 0.01 and the background magnetic field B_0 is 1.291 (resonance condition). The first 1 t_a is taken out in figure 3.a and ran again with finer time resolution (0.001 t_a). After that, in order to estimate the true growth rate of $\delta\rho_{2,rms}$, a sliding window is used to demonstrate the local oscillation of growth rate due to the edge effect introduced by the finite size of simulation box. And lastly, a period is selected manually to estimate the averaged growth rate with the following two criteria: (1) The key feature of oscillation shows no or minimum alternations in the selected period. (2) The period is near the start of this simulation (because the growth rate is expected to decrease as $\delta\rho_{2,rms}$ increases, due to conservation of energy). The result is the dashed green line in figure 5 and for comparison, the theoretical result is shown as the red dashed line.

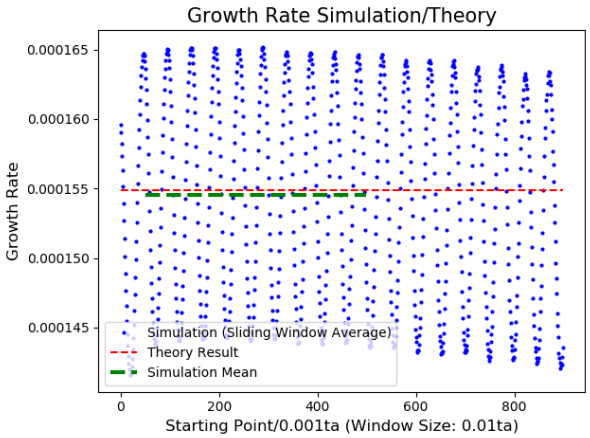

Figure 5: Resonance growth rate estimated from sliding window. Sliding window size is 100 data points, which in this case, is 0.1 t_a.

As can be found in figure 5, due to the edge effect of the simulation box introduced during the calculation of $\delta\rho_{2,rms}$ in (38) (or maybe it's something else? Might not be this trivial), the growth rate oscillates in a manner in accordance with sin or cos (not surprisingly). The green dashed line indicates the averaged growth rate estimated using the period spanned by itself. Result shows that the simulation result coincides nearly perfectly with the theoretical result with a relative error far less than 1%. This is expected due to the fact that during resonance, second order effect dominates as opposed to the non-resonant case, the behavior of second order effects themselves has a phase shift and numerous other effects that can significantly alter the behaviors of themselves.